

Development of Near-Infrared-Emitting Scintillators Based on Rare-Earth-Doped Garnet Crystals—Part 1

Go Okada,* Noriaki Kawaguchi, and Takayuki Yanagida

Graduate School of Materials Science, Nara Institute of Science and Technology (NAIST),
8916-5 Takayama, Ikoma, Nara 630-0192, Japan

(Received March 27, 2017; accepted July 13, 2017)

Keywords: near-infrared, scintillator, $Y_3Al_5O_{12}$ (YAG), $Y_3Al_2Ga_3O_{12}$ (YAGG)

In this paper, we report on experimental results towards the development of near-infrared (NIR)-emitting scintillators based on rare-earth-doped garnet crystals, which were obtained as a part of collaborative research with the Nuclear Power Safety Technology Research Center, Chubu Electric Power Co., Inc. A series of garnet scintillators, $Y_3Al_5O_{12}$ (YAG) and $Y_3Al_2Ga_3O_{12}$ (YAGG) doped with rare-earth elements (Nd, Sm, Ho, Er, Tm, and Yb) at varying concentrations (0.5, 1.0, 2.0, 5.0, and 10.0 mol%), were synthesized by the floating zone method and systematically characterized for NIR-emitting scintillator applications. Among all the samples, 5% Nd-doped YAG showed the highest scintillation intensity (integration mode). By taking the spectral responsivity of the photodetector and the attenuation of optical light guide into consideration, a combination of 5% Yb-doped YAG and an InGaAs detector is expected to give the highest detectable signal. The scintillation intensity effectively depends on the photoluminescence quantum yield and energy transfer efficiency, which is effectively correlated with not the quality of the crystal but the type of rare-earth ion doped.

1. Introduction

Measurements of ionizing radiation⁽¹⁾ have been demanded for a wide range of application fields such as medicine, security, and astronomy. The field of energy dealing with, for example, nuclear power generation is not an exception. Scintillators are often used for radiation measurements as they convert radiation into low-energy photons, which are measurable by conventional photodetectors. As a detector assembly, the scintillator may be attached directly on a photodetector in order to collect the scintillation photons most efficiently, or it can be attached to a light guide, e.g., optical fibre, coupled with a photodetector so that radiation can be measured remotely and online, as sketched in Fig. 1. The latter measurement configuration has also an advantage, that is, a power supply and other electronic devices are not required at the measurement site; therefore, it is especially preferable for measuring high radiation fields in a restricted area. For such applications, scintillators emitting near-infrared (NIR) light^(2,3) are preferably used mainly for the following two reasons. (1) Under high-radiation fields, optical fibres suffer radiation damage, which appear as a change in colour owing to the radiation-induced absorption in the ultraviolet (UV) and visible wavelength regions. (2) Under high-radiation fields, Cherenkov light emerges in the UV and

*Corresponding author: e-mail: go-okada@ms.naist.jp
<http://dx.doi.org/10.18494/SAM.2017.1620>

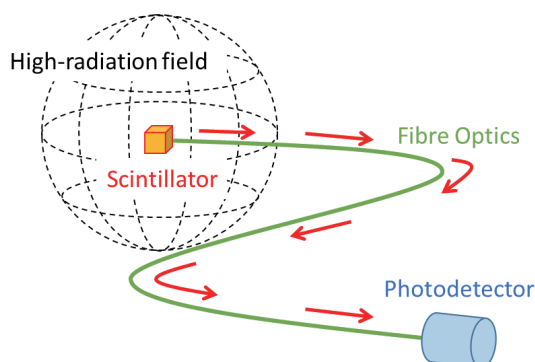


Fig. 1. (Color online) Schematic diagram of radiation measurement configuration using a scintillator coupled with fibre optics.

visible ranges and contributes as noise if the scintillation light is in the same spectral range. In addition, NIR-emitting phosphors have been intensively studied for bio-imaging applications in recent years.^(4–11)

Rare-earth-doped garnet materials are of considerable interest as scintillator materials. There are a number of rare-earth-doped garnet scintillators commercially available,^(12–17) and they are characterized as having a considerably high scintillation intensity among oxide scintillators. However, the emission range of conventional scintillators is in the UV and visible range under the assumption that they will be used together with a photomultiplier tube (PMT) in the counting mode. In earlier research, Takada *et al.* tested the fibre-coupled configuration and confirmed the detection capability using red-NIR emission of a Pr-doped $\text{Gd}_2\text{O}_2\text{S}$ (GOS:Pr) scintillator with Si-based CCD detection in the integration mode and experimentally confirmed the measurement capability of as low as 0.8 Gy/h.⁽¹⁸⁾ Towards the goal of developing bright NIR-emitting scintillators based on garnet crystals, we have been conducting a two-year project as collaborative research with the Nuclear Power Safety Technology Research Center, Chubu Electric Power Co., Inc. In this paper, we report the experimental data obtained during the first-half of the project.

2. Materials and Methods

A series of rare-earth-doped garnet crystals were synthesized by the floating zone (FZ) method. The crystals studied in this research are two types of garnet hosts, $\text{Y}_3\text{Al}_5\text{O}_{12}$ (YAG) and $\text{Y}_3\text{Al}_2\text{Ga}_3\text{O}_{12}$ (YAGG), doped with six different rare-earth ions (Nd, Sm, Ho, Er, Tm, and Yb) at five different concentrations (0.5, 1.0, 2.0, 5.0, and 10.0 mol%); thus, 60 different samples were studied in total. These rare-earth ions were selected as they are commonly known to show NIR luminescence. A diffractometer (Miniflex 600, Rigaku) was used to investigate the crystal structure using a $\text{Cu}(\text{K}\alpha)$ X-ray source. The scintillation emission spectrum was measured using a laboratory-made setup. The sample was irradiated with X-rays from the generator (Monoblock XRB80N100, Spellman) inside an integrated sphere (4P-GPS-060-SF, Labsphere) attached with an optical fibre. The X-ray generator was equipped with a conventional X-ray tube having a W anode and a Be window. The applied acceleration voltage was 80 kV while the tube current was 1.2 mA. The scintillation light is guided to two different CCD-based spectrometers – Ocean Optics QE Pro for the UV and visible ranges and Andor DU492A-1.7 iDus InGaAs for the NIR range. The absolute photoluminescence (PL) quantum yield (PLQY) was measured using Hamamatsu Quantaaurus-QY (C11347). Since the instrument only offers measurement shorter than 800 nm,

PLQY including emissions of longer wavelength was calculated using a complete PL spectrum over the entire spectral range fitted with the data measured with the instrument.

3. Experimental Results

Figure 2 illustrates selected garnet crystal samples synthesized in this study. The typical size of the obtained crystals is ~ 3 mm in diameter and 15–30 mm in length. For the optical absorption of rare-earth elements included, the samples are coloured and the strength depends on the concentration of doped rare-earth elements. Some crystal samples are not transparent owing to the inclusion of a significant number of cracks.

Figure 3 shows powder X-ray diffraction (XRD) patterns of selected samples. The standard patterns from the Cambridge Structural Database for YAG (CSD4312143) and YAGG (CSD2003069)

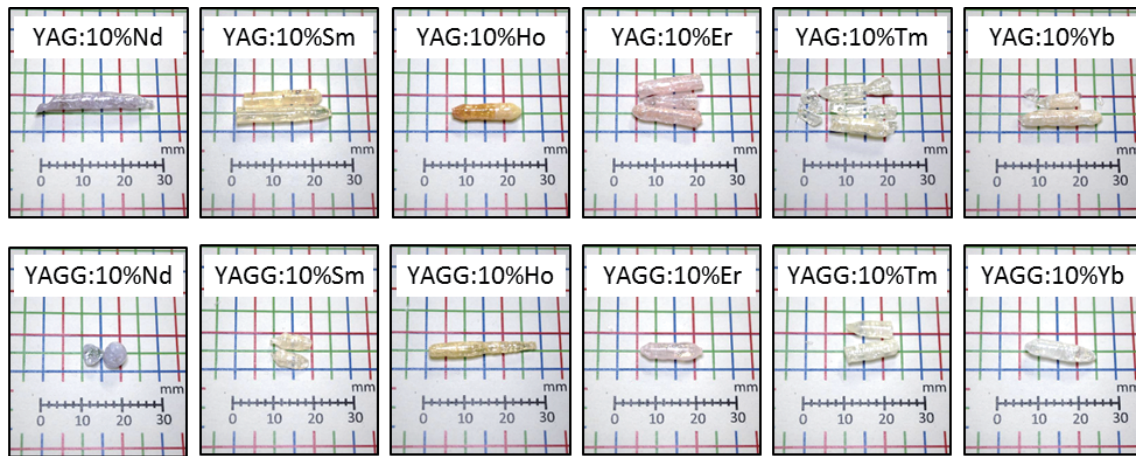


Fig. 2. (Color online) Representative garnet crystals synthesized. Those on the top and bottom rows are YAG and YAGG crystals, respectively. The rare-earth ions doped and their concentrations are indicated in the images.

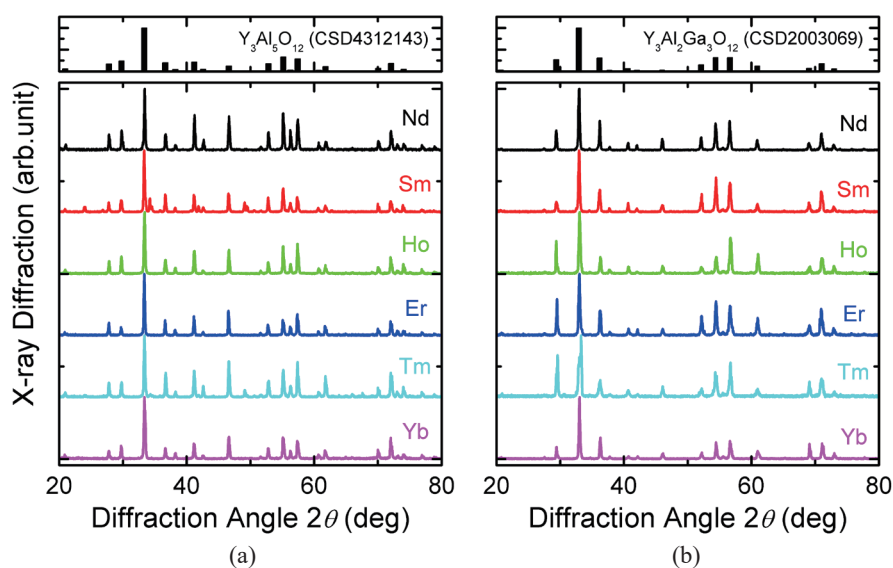


Fig. 3. (Color online) Representative powder XRD patterns of (a) YAG and (b) YAGG samples. Doping concentrations are fixed at 2.0%. Standard patterns of YAG and YAGG from the Cambridge Structural Database are also illustrated.

are also illustrated together. All the measured patterns are in agreement with the standard pattern of the corresponding host material; therefore, we have confirmed that the intended crystals were successfully obtained.

The qualities of the crystal samples were evaluated using the broadening of the X-ray diffraction peak as a figure of merit. The diffraction peak of interest was that of the $(h k l) = (4 2 0)$ crystal plane at around $2\theta = 33.5^\circ$. The subsequent diffraction peak for each sample was fitted by a sum of two Lorentzians as

$$I(2\theta) = I_1 \left[\frac{\gamma^2}{(2\theta - 2\theta_1)^2 + \gamma^2} \right] + I_2 \left[\frac{\gamma^2}{(2\theta - 2\theta_2)^2 + \gamma^2} \right], \quad (1)$$

where 2θ is the diffraction angle, I_1 and I_2 are diffracted peak intensities of $\text{CuK}\alpha_1$ and $\text{CuK}\alpha_2$ X-rays centering at diffraction angles of $2\theta_1$ and $2\theta_2$, respectively, and γ is diffraction peak broadening, which is considered to be a crystallinity factor. For analyses, the contribution of instrumental broadening for γ is subtracted from the experimental data, and the instrumental broadening was measured using a Si standard powder sample. Figure 4 shows the crystallinity factors (γ) of YAG and YAGG crystals as functions of doping concentration and doping element. The qualities of YAG samples seem to be higher than those of YAGG as the mean value is smaller, $\bar{\gamma}(\text{YAG}) = 6.4 \times 10^{-3}$ (deg) and $\bar{\gamma}(\text{YAGG}) = 3.3 \times 10^{-2}$ (deg). In particular, dependences on the dopant concentration and element are reasonably represented for YAGG, while no strong dependence is observed for YAG samples as the values are small and equivalent to the measurement errors.

Figure 5 shows the PLQY of YAG and YAGG crystals as a function of concentration and dopant element. The data indicated in circles are mean values while the error bars indicate deviations of statistical matrix groups. For both YAG and YAGG, the PLQY seems to decrease with increasing dopant concentration owing to concentration quenching. In contrast, the PLQY is strongly dependent on the type of rare-earth element doped. Among the present samples, the PLQY is relatively high for Nd, Sm, and Yb. Comparison between YAG and YAGG shows that the difference is not significant but YAGG seems to show a slightly higher value (68.8% on average) than YAG (67.5% on average).

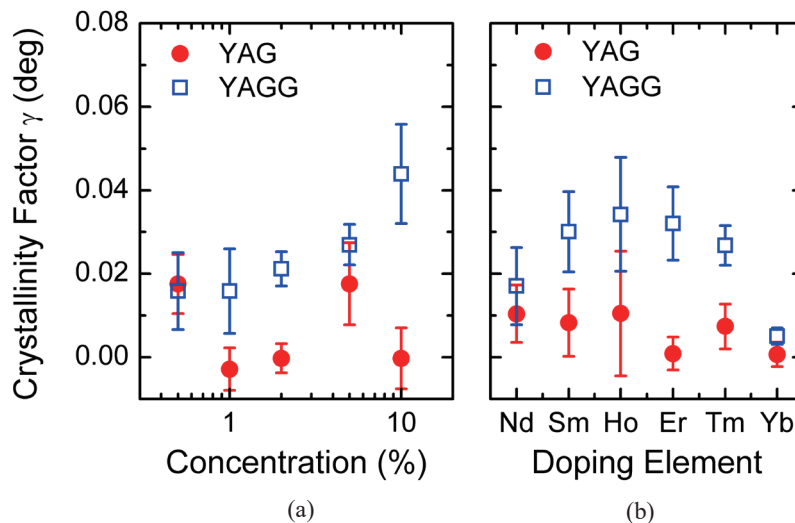


Fig. 4. (Color online) γ of YAG and YAGG crystal samples as functions of (a) concentration and (b) dopant type.

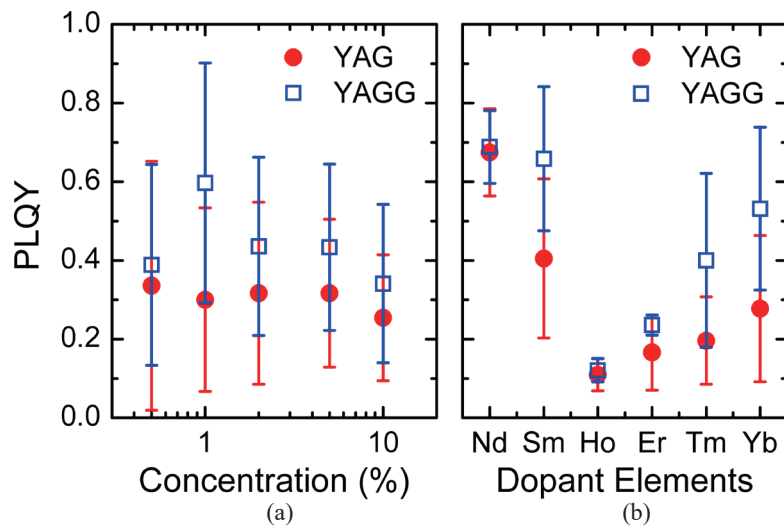


Fig. 5. (Color online) PLQY of rare-earth-doped YAG and YAGG as functions of (a) concentration and (b) dopant element.

Figure 6 shows scintillation spectra of selected YAG and YAGG samples doped with a series of rare-earth ions. All the samples show measurable signals but the intensity and the spectrum strongly vary. The emission is mainly due to the 4f–4f transitions of the rare-earth ions doped. Figure 7 summarizes integrated scintillation intensities over the entire spectral range of measurement for all the prepared samples. For qualitative comparison, the intensities are normalized to the unit volume. The data indicated in circles are the average values while the error bars indicate deviations. For reference, the integrated scintillation intensity of the commercial GOS:Pr scintillator (LS-1, Hitachi Metals) is represented as dashed lines. For both YAG and YAGG, the scintillation intensity seems to increase with increasing concentration of rare-earth dopants. However, comparison between the 5.0%- and 10.0%-doped samples shows that the 10.0%-doped ones show lower intensities, which may be due to concentration quenching. Regarding the type of rare-earth dopants, Nd-, Sm-, and Yb-doped samples show stronger luminescence than those doped with Ho, Er, and Tm, by a factor of approximately 4–5 for YAG and ~10 for YAGG. Comparison between YAG and YAGG shows that the mean intensity of YAG-based samples is slightly higher by a factor of 2.4. Among all the samples, 5%-Nd-doped YAG shows the highest scintillation intensity.

4. Discussion

In the current application of interest, scintillation light propagated through optical fibres is detected by a photodetector (Fig. 1). Therefore, the detected signal strongly depends on the spectral responsivity of the detector and attenuation coefficients of the fibre. To evaluate the scintillation signal intensity to be detected, one must consider the contribution of those two parameters. Thus, the detectable signal (I) can be simulated by

$$I = \int_{600}^{1600} I_0(\lambda) \times 10^{\frac{-\alpha_{dB}(\lambda)L}{10}} \times R(\lambda)d\lambda, \quad (2)$$

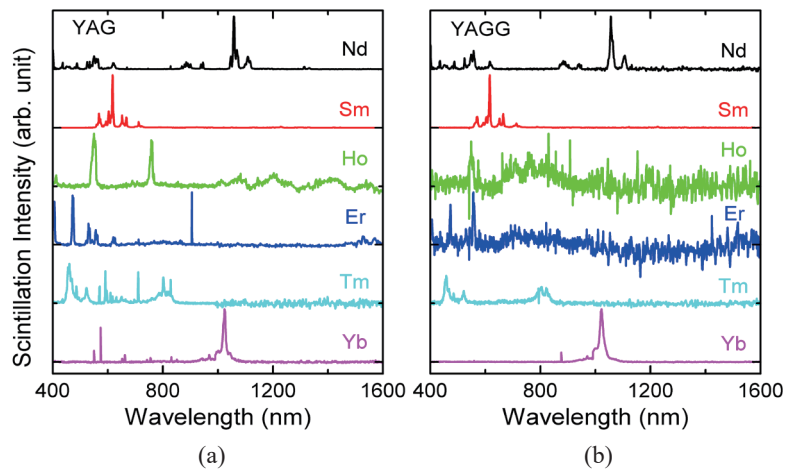


Fig. 6. (Color online) Representative scintillation spectra of (a) YAG and (b) YAGG samples. Doping concentrations are fixed to 5.0%.

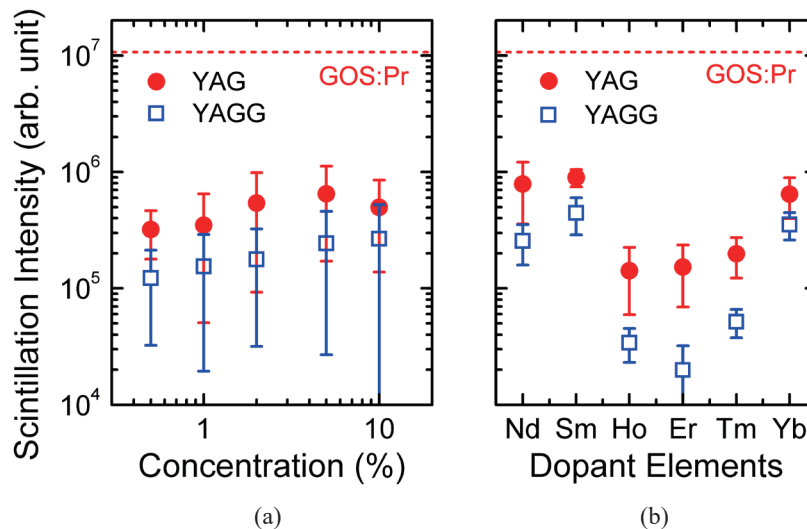


Fig. 7. (Color online) Integrated scintillation intensities of YAG and YAGG samples as a function of (a) concentration and (b) doping element. The dashed lines represent the values for the GOS:Pr scintillator.

where $I_0(\lambda)$ is the scintillation intensity per unit volume as a function of wavelength λ , $\alpha_{dB}(\lambda)$ is the attenuation coefficient of the optical fibre, L is the length of the optical fibre, and $R(\lambda)$ is the responsivity of the photodetector. In this simulation, a common silica fibre of 30 m length is used.⁽¹⁹⁾ Figure 8 represents the detectable signals simulated for the rare-earth-doped YAG crystal samples. The simulations were performed for three different photodetectors with different responsivity profiles: the PMT (H7422, Hamamatsu), avalanche photodiode (APD; S11519, Hamamatsu), and InGaAs detector (iDus InGaAs 1.7 μm , Andor). When the PMT is used, Sm-doped samples seem to be the most appropriate as they have reasonably high intensity together with a shorter emission wavelength. (The overall detectable signal with the PMT is much smaller than the others by more than two orders of magnitude because the selected PMT has a low responsivity at the cost of increasing sensitivity in the NIR region.) With APD and InGaAs detectors, Yb-doped samples are

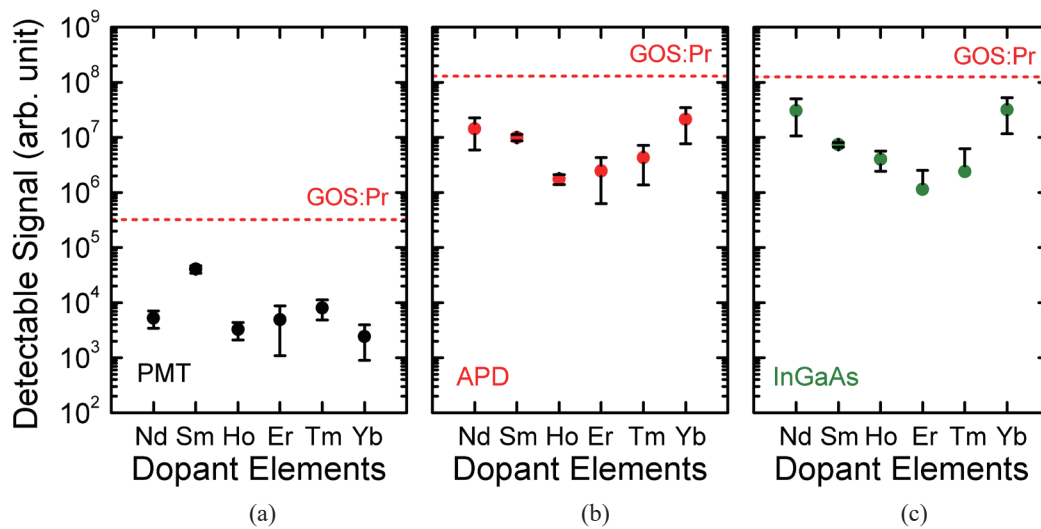


Fig. 8. (Color online) Detectable scintillation signals of YAG samples using different photodetectors: (a) PMT, (b) APD, and (c) InGaAs.

the best to be used. Among all the combinations of a photodetector and scintillator sample, 5.0% Yb-doped YAG with the InGaAs detector showed the highest detectable signal. However, the latter intensity is still lower by a factor of approximately 2 compared with GOS:Pr with the APD detector. Thus, further improvement of scintillation intensity should be considered.

Figure 9 summarizes the scintillation intensities of rare-earth-doped YAG and YAGG crystal samples as a function of PLQY, γ , and S , which was derived on the basis of Robbins' model,^(20–22)

$$\eta = \beta \cdot S \cdot Q, \quad (3)$$

where η is the scintillation efficiency (equivalent to light yield), β is the efficiency of generating electron-hole pairs, and Q is PLQY. A qualitative factor for S is given from the above equation since η is the equivalent for scintillation intensity for a fixed incident energy and host matrix, β is constant for the same host matrix,⁽²⁴⁾ and Q is known from the experiment. In the figures, the least-squares fit of experimental data with a power function and the R -squared value are also presented in order to evaluate the degree of correlation. On one hand, as predicted by Robbins' model, the scintillation intensity is reasonably correlated with the PLQY and S . On the other hand, no effective correlation with γ is observed for either YAG or YAGG. In fact, the latter observation is interesting because it is generally understood that S is higher for a higher degree of crystallinity or smaller γ . One may wonder what determines S in the present system. Figure 10(a) shows S as a function of γ . It is clearly demonstrated that S and γ are not effectively correlated and the R -squared values are very small. However, S seems to be reasonably correlated with the type of rare-earth element doped, as demonstrated in Fig. 10(b). Note that the order on the horizontal axis is not the same as in Figs. 7 and 8 (atomic number). These observations suggest that S in the rare-earth-doped YAG and YAGG crystals more strongly depends on the type of rare-earth element doped than the quality of the crystal host. One possible interpretation is that there exist certain barriers between the host matrix and the doped rare-earth element preventing energetic electrons and holes propagating in the host from being transferred and emitting light at the rare-earth centres. The

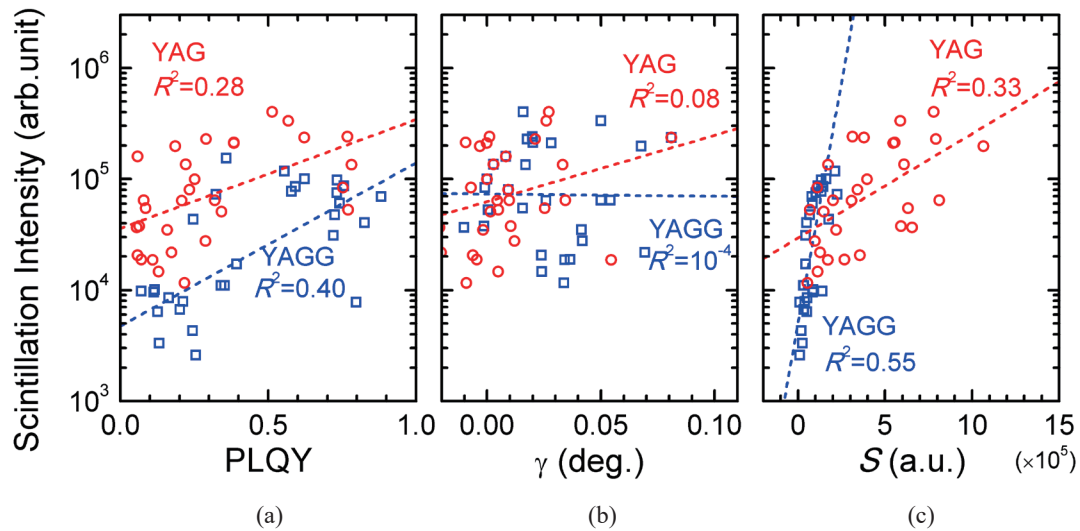


Fig. 9. (Color online) Scintillation intensities of rare-earth-doped YAG and YAGG crystals as a function of (a) PLQY, (b) γ , and (c) S .

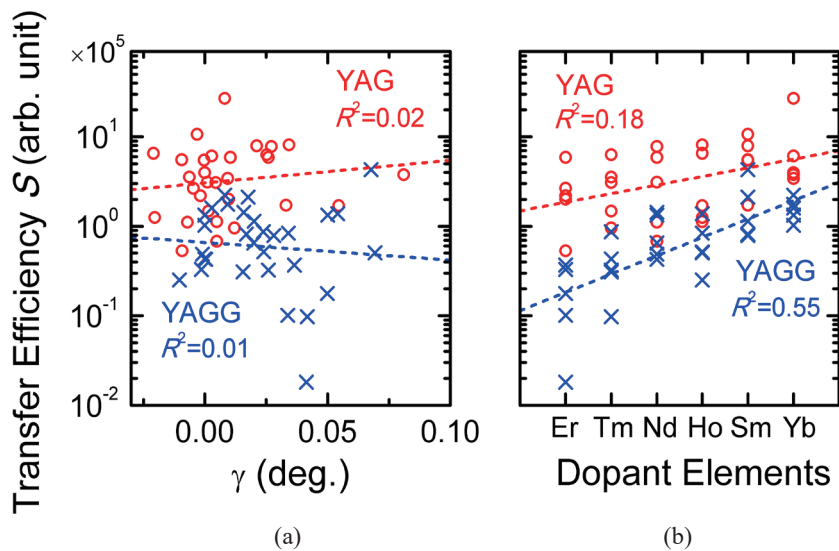


Fig. 10. (Color online) S vs (a) γ and (b) dopant elements for YAG and YAGG.

origin of such barriers is currently unknown. In addition, it should be mentioned here that garnet-type crystals commonly include some defects, such as F-type centres and antisites, that act as emission centres and show luminescence in the UV region. The energy consumed as the latter luminescence may affect S . We, however, could not observe such emission, most likely because of insufficient detector sensitivity. Further investigation is required in order to enhance and optimize the scintillation properties.

5. Conclusions

We developed 60 different garnet crystals with two different crystal hosts (YAG and YAGG) doped with six different rare-earth ions (Nd, Sm, Ho, Er, Tm, and Yb) at five different concentrations (0.5, 1.0, 2.0, 5.0, and 10.0%). The prepared samples were characterized in consideration of applications as NIR-emitting scintillators. Among the samples developed, Nd-, Sm-, and Yb-doped samples showed effective high scintillation intensities; however, the intensities were much lower than that of the GOS:Pr scintillator. The scintillation intensity is dependent on the PLQY and energy transfer efficiency, which is effectively correlated with not the quality of the crystal but the type of rare-earth ion doped. Further developments will continue to improve the scintillation intensity of NIR-emitting scintillators based on rare-earth-doped garnet crystals.

Acknowledgments

This research was performed as a collaborative project with the Nuclear Power Safety Technology Research Center, Chubu Electric Power Co., Inc., who also provided financial support to carry out the experimental works in this project.

References

- 1 G. F. Knoll: Radiation Detection and Measurement, 4th ed. (Wiley, New York, 2010).
- 2 T. Oya, G. Okada, and T. Yanagida: *J. Ceram. Soc. Jpn.* **124** (2016) 536.
- 3 D. Nakauchi, G. Okada, M. Koshimizu, and T. Yanagida: *J. Rare Earths* **34** (2016) 757.
- 4 C. L. Amiot, S. Xu, S. Liang, L. Pan, and J. X. Zhao: *Sensors* **8** (2008) 3082.
- 5 K. Soga, T. Tsuji, F. Tashiro, J. Chiba, M. Oishi, K. Yoshimoto, Y. Nagasaki, K. Kitano, and S. Hamaguchi: *J. Phys. Conf. Ser.* **106** (2008) 12023.
- 6 J.-L. Boulnois: *Lasers Med. Sci.* **1** (1986) 47.
- 7 J. Xu, D. Murata, J. Ueda, and S. Tanabe: *J. Mater. Chem. C* **4** (2016) 11096.
- 8 Y. Katayama, B. Viana, D. Gourier, J. Xu, and S. Tanabe: *Opt. Mater. Express* **6** (2016) 1405.
- 9 Y. Katayama, H. Kobayashi, J. Ueda, B. Viana, and S. Tanabe: *Opt. Mater. Express* **6** (2016) 1500.
- 10 J. Xu, J. Ueda, and S. Tanabe: *Opt. Mater. Express* **5** (2015) 963.
- 11 J. Xu, J. Ueda, Y. Zhuang, B. Viana, and S. Tanabe: *Appl. Phys. Express* **8** (2015) 42602.
- 12 T. Yanagida, H. Takahashi, T. Ito, D. Kasama, T. Enoto, M. Sato, S. Hirakuri, M. Kokubun, K. Makishima, T. Yanagitani, H. Yagi, T. Shigeta, and T. Ito: *IEEE Trans. Nucl. Sci.* **52** (2005) 1836.
- 13 T. Yanagida, K. Kamada, Y. Fujimoto, H. Yagi, and T. Yanagitani: *Opt. Mater.* **35** (2013) 2480.
- 14 T. Yanagida, Y. Fujimoto, M. Koshimizu, K. Watanabe, H. Sato, H. Yagi, and T. Yanagitani: *Opt. Mater.* **36** (2014) 2016.
- 15 M. Mori, J. Xu, G. Okada, T. Yanagida, J. Ueda, and S. Tanabe: *J. Rare Earths* **34** (2016) 763.
- 16 T. Yanagida, Y. Fujimoto, Y. Yokota, K. Kamada, S. Yanagida, A. Yoshikawa, H. Yagi, and T. Yanagitani: *Radiat. Meas.* **46** (2011) 1503.
- 17 M. Mori, J. Xu, G. Okada, T. Yanagida, J. Ueda, and S. Tanabe: *J. Ceram. Soc. Jpn.* **124** (2016) 569.
- 18 E. Takada, A. Kimura, Y. Hosono, H. Takahashi, and M. Nakazawa: *J. Nucl. Sci. Technol.* **36** (1999) 641.
- 19 E. F. Schbert: *Light-Emitting Diodes* (Cambridge University Press, Cambridge, 2006).
- 20 D. J. Robbins: *J. Electrochem. Soc.* **127** (1980) 2694.
- 21 A. Lempicki, A. J. Wojtowicz, and E. Berman: *Nucl. Inst. Methods Phys. Res., Sect. A* **333** (1993) 304.
- 22 C. L. Å. Melcher: *Nucl. Instrum. Methods Phys. Res., Sect. A* **537** (2005) 6.
- 23 P. Dorenbos: *Nucl. Instrum. Methods Phys. Res., Sect. A* **486** (2002) 208.